Doklady Earth Sciences, Vol. 395A, No. 3, 2004, pp. 378–384. Translated from Doklady Akademii Nauk, Vol. 395, No. 4, 2004, pp. 517–523.

GEOCHEMISTRY

Mineralogy and Geochemistry of Mantle Inclusions and Mantle Column Structure of the Yubileinaya Kimberlite Pipe, Alakit Field, Yakutia

I. V. Ashchepkov[1], N. V. Vladykin[2], I. V. Nikolaeva[1], S. V. Palessky[1], A. M. Logvinova[1], A. I. Saprykin[1], O. S. Khmel'nikova[1], and G. N. Anoshin[1]

Presented by Academician N.L. Dobretsov June 9, 2003

Received June 30, 2003

The mantle column structure has been defined only for the Udachnaya [1] and Mir [2] kimberlite pipes of the Siberian Platform. Peridotite xenoliths are generally serpentinized. However, their concentrate contains not only resistant minerals (garnet, ilmenite, chromite, zircon, and rutile), but also pyroxenes. This paper is based on more than 700 microprobe analyses, including more than 200 analyses of peridotite clinopyroxenes and amphiboles from the Yubileinaya Pipe (table). These data have made it possible to reconstruct the mantle column.

Mantle clinopyroxenes, garnets, Cr-spinels, ilmenites, and micas from more than 20 samples were analyzed by LAM ICP-MS on a high-resolution ELEMENT Finnigan mass spectrometer using a Nd-YAG laser (UV laser probe, wavelength 266 nm) and NIST SRM 612 standard in the Analytical Center of the Joint Institute of Geology, Geophysics, and Mineralogy, Novosibirsk. The detection limit is 10–100 ng/g.

Like their counterparts from the heavy concentrate in Colorado and micaceous kimberlites in the Daldyn field [4], Cr-diopsides from this pipe have high Na_2O (up to 5%) and Cr_2O_3 (up to 6%) contents (Fig. 1a). The scarce pyroxenes with low Na_2O, Al_2O_3, and Cr_2O_3 contents are similar to pyroxenes from garnet peridotites, while the high-Al pyroxenes are similar to those from spinel peridotites of the Udachnaya Pipe [1]. Augites and salites were entrapped from crustal and cumulus rocks.

Pyropes from the Yubileinaya Pipe form an extended trend up to 12 wt % Cr_2O_3. The Cr-free pyropes (Fig. 1) are typical of eclogites, pyroxenites, and megacrysts. As is the case in most kimberlite pipes, the inflection of lherzolite pyrope field at 4–5 wt % Cr_2O_3 [5] (Fig. 1b, trend *2*) reflects the lithological boundary between garnet–spinel (Fig. 1b, *2*) and garnet peridotites of the diamond facies (*3*). The high-Ti garnets are probably derived from pyroxenites (*7*). The subcalcic garnets (*9, 10*) are separated by trend (*8*) along the boundary of the lherzolite field from garnets at the upper boundary (groups *4–6*).

In terms of Cr_2O_3 content variation from 63 to 10 wt % (Fig. 1c), chromites can be divided into intervals that correlate with garnet groups. The four clusters with the highest Cr concentration are characterized by different grades of enrichment in TiO_2 and FeO. Thus, they form divergent trends with a maximum deviation from the mantle array for dunites–harzburgites and high-Al chromites. Figure 1d shows the ilmenite trend (TiO_2 56–44 wt %), which is typically considered a result of fractionation [6]. However, the simultaneous increase of FeO and Cr_2O_3 suggests the AFC mechanism [7] with chromite dissolution at the late crystallization stages. The ilmenite trend includes groups *6* and *7*, with high dispersions of the Cr_2O_3, Al_2O_3, V_2O_5, and NiO contents in each group. The sharp divide at 50% TiO_2 into low- and high-Al varieties presumably implies different proportions of coherent crystallizing (or assimilated) garnet.

The moderate FeO enrichment (4–6 wt %) and simultaneous decrease of TiO_2 and Cr_2O_3 (Fig. 1e) in the phlogopites can be related to joint crystallization of rutile, which is included in many grains, and the increase of the eastonite end member typical of micas

[1] *United Institute of Geology, Geophysics, and Mineralogy, Siberian Division, Russian Academy of Sciences, pr. akademika Koptyuga 3, Novosibirsk, 630090 Russia; e-mail: Igor.Aschepkov@uiggm.nsc.ru*

[2] *Vinogradov Institute of Geochemistry and Analytical Chemistry, Siberian Division, Russian Academy of Sciences, ul. Favorskogo 1a, Irkutsk, 664033 Russia*

from shallow zones [8]. Magnesian phlogopites are lower in TiO_2 and Cr_2O_3. Micas with a higher Fe concentration are similar to glimmerite varieties. The Fe–Ti varieties are close to megacrysts from alkaline basalts. The high-Fe varieties are related to the magmatic (kimberlitic) process. The amphiboles can be divided into five groups. The increase of FeO and Al_2O_3 (Fig. 1f) corresponds to the transition from deep-seated richterite–cataphorites to shallow pargasites and pargasite hornblendes with a Cr_2O_3 content of ~1–2%.

Clinopyroxene thermobarometry [9] calculated *PT* values for ~200 grains allowed us to construct a geotherm, the cold branch of which is close to 37 mW/m^2, while the main branch corresponds to a heat flow of 40 mW/m^2 (Fig. 2b). The geotherm calculated using a new version of a Jd–Di barometer [10] is more regular and closer to 40 mW/m^2 (Fig. 1a). Since the thermometer [9] underestimates temperature for high-Na pyroxenes, we applied a polynomial approximation with estimations based on an orthopyroxene thermometer [10]. Thermobarometric models yield somewhat different *TP* intervals. Version [10] provides a more detailed subdivision. Figure 2a shows that the section can be divided into the following units: (1) a heated asthenospheric unit (tectonized peridotites) [1, 11]; (2) unevenly heated dunite–harzburgites (Fig. 1b, *9, 10*); (3–5) three units of diamond-facies peridotites, which may correspond to the respective three garnet groups (*4–6*), (6) metasomatic pyroxenites that usually define the inflection in Cr_2O_3–CaO trend for garnet (*3, 4, 7*); (7) garnet–spinel peridotites (*2*); and (8) spinel peridotites. Black pyroxenes correspond to middle–lower crustal cumulates with temperatures of ~1050–1150°C. Clinopyroxene and garnet inclusions in diamonds correspond to the two lower units.

The pyroxenes from four pressure intervals exhibit nearly straight subparallel REE patterns with high $(La/Yb)_n$ ratios. Their spidergrams are characterized by Th–U enrichment, Nb–Ta and Pb anomalies correlating with Na and Cr concentrations and depths calculated after [9, 10], and depletion in Cs and Rb relative to LREE-poor varieties with insignificant Ce minimums (Fig. 3). The asymmetric hump-shaped REE pattern typical of garnet peridotites and Ta–Nb peaks were found only for pargasite amphibole. Phlogopite has a fractionated pattern with HFSE and Rb enrichment. In garnets, Cr_2O_3 (10–3 wt %) shows a negative correlation with HREE. The deeper-seated garnets have an S-shaped REE pattern, insignificant Th and U peaks, and Ti minimums. The Pb maximums and Sr minimums are typical of all garnets, while low-Cr garnets are enriched in TiO_2. Ilmenites are characterized by W-shaped REE patterns, which have a negative correlation with Nb, Ta, Zr, Hf, and Ti peaks. Relative to ilmenites, two chromite samples have lower HREE concentrations and insignificant Nb, Ta, Ti, and U peaks.

Calculations of distribution coefficients show that the deep-seated (mainly subcalcic) garnets with the highest Cr concentration and pyroxenes were derived from similar melts enriched in Th–U and depleted in HFSE. Parental melts for ilmenite and chromite are distinguished from those for garnet and clinopyroxene in their lower $(La/Yb)_n$ and W-shaped pattern, which is possibly related to the chromatographic effect. The similarity of the geochemical features suggests that the ilmenites at the end of trend could be crystallized by the AFC mechanism [7] with chromite dissolution. It should be noted that the kimberlite fields and pipes in the Yakutian province differ in the geochemistry of ilmenites, chromites, and other minerals.

The data presented above allow us to suggest the following hypothetical model of mantle column formation in the Yubileinaya Pipe: Discrete mineral trends suggest that the layered structure of the mantle section (based on thermobarometric reconstructions) is related to subduction [9]. Relatively low-Cr dunite–harzburgite garnets presumably overlying the asthenospheric unit, which is represented by pyroxenes close to tectonized peridotites [1, 11], are recorded twice within the interval of 60–40 kbar. This is confirmed by the presence of three lherzolite garnet clusters. The garnets are presumably overlain by no fewer than three peridotite lenses. The LILE and Th enrichment of peridotites from the lower units implies a contribution of the mature crustal material and large-scale metasomatism with HFSE depletion. The similar compositions of pyroxenes from inclusions in Namibian diamonds [12] associated with carbonates indicate a possible carbonatite metasomatism.

The amphibole and phlogopite compositions indicate that metasomatism of the upper section with Ti, Ca, Fe, and Al enrichment at >35 kbar was similar to the interaction with plume melts–fluids. Based on the occurrence frequency, metasomatites are mainly restricted to the intermediate *TP* interval marked by a change in rock geochemistry. The pressure interval 35–40 kbar, which marks the change in mantle lithology and the graphite–diamond transition, also represents the level of dehydration of the peridotite mantle wedges of subducted slabs [13]. It is traced by metasomatites and anatectic pyroxenites. This level also marks the interaction between plume melts and peridotites [3, 14], which is often accompanied by delamination [14] of the lower (eclogitized) part of the mantle keel. Metasomatism in the lower mantle column may be related to plumes or early subduction stages. The carbonatite metasomatism is possibly coeval or conjugated with the development of conduits and intrusion of kimberlites. An analogy with megacryst assemblage of alkaline basalts [15] suggests that megacrysts of garnet, picroilmenite, and pyroxene crystallized at different pressures during the formation of kimberlite conduits. At the

Table 1. Composition of representative minerals from concentrate of the Yubileinaya kimberlite pipe

Component	1	2	3	4	5	6
SiO_2	41.00	41.21	41.63	41.09	39.47	–
TiO_2	0.03	0.24	0.84	0.12	0.35	48.09
Al_2O_3	16.34	18.30	19.28	19.36	14.56	0.45
Cr_2O_3	9.52	6.50	3.92	5.40	10.14	0.91
FeO	6.95	6.95	8.36	6.77	6.43	39.80
MnO	0.52	0.37	0.31	0.40	0.43	0.27
MgO	20.90	20.22	20.55	21.82	19.70	9.21
CaO	3.64	4.50	4.99	3.23	4.31	0.02
Na_2O	0.04	0.07	0.07	0.07	0.17	–
K_2O	–	–	–	–	–	0.05
Total	98.94	98.36	99.95	98.26	95.55	98.81
Ba	0.89	0.45	0.79	0.43	0.67	0.44
La	0.15	0.05	0.03	0.02	0.16	0.03
Ce	0.61	0.14	0.10	0.11	0.29	0.044
Pr	0.13	0.03	0.02	0.02	0.08	0.008
Nd	1.00	0.41	0.23	0.27	0.47	0.059
Sm	0.37	0.27	0.20	0.16	0.51	0.060
Eu	0.10	0.10	0.07	0.07	0.27	0.034
Gd	0.25	0.44	0.30	0.21	1.14	0.073
Tb	0.01	0.07	0.05	0.04	0.20	0.016
Dy	0.08	0.42	0.31	0.15	1.12	0.068
Ho	0.01	0.10	0.06	0.02	0.18	0.011
Er	0.04	0.29	0.15	0.05	0.35	0.034
Tm	0.01	0.05	0.02	0.00	0.04	0.004
Yb	0.07	0.25	0.17	0.06	0.26	0.017
Lu	0.01	0.05	0.03	0.02	0.04	0.005
Hf	0.17	0.10	0.22	0.10	0.31	4.1
Ta	0.02	0.01	0.02	0.00	0.02	58.1
Pb	0.30	0.16	0.27	0.10	0.33	0.12
Th	0.07	0.02	0.02	0.01	0.08	0.006
U	0.03	0.01	0.01	0.01	0.02	0.014
V	27	45	39	36	73	628
Sc	28.8	24.3	16.5	22.1	51.1	14.8
Co	29.8	27.7	22.7	19.5	23.2	82.7
Cu	7.0	6.6	6.6	6.7	7.1	14.1
Ni	553	292	476	312	460	5180
Rb	40	19.98	5.12	0.334	0.380	0.44
Sr	1.80	1.09	0.96	0.72	3.65	0.69
Y	0.30	2.73	1.61	0.59	4.72	0.33
Zr	2.2	3.7	7.9	6.0	24.5	126
Nb	0.21	0.10	0.10	0.07	0.25	415
Cs	0.008	0.008	–	–	0.004	0.002

Notes: Major components were analyzed on a Camebax Micro microprobe (O.S. Khmel'nikova, analyst). Trace elements were analyzed by LAM ICP-MS in the Analytical Center of the United Institute of Geology, Geophysics, and Mineralogy, Novosibirsk (I.V. Nikolaeva, S.V. Palesskii, and A.I. Saprykin, analysts). Minerals: (1–5) Garnet, (6–7) ilmenites, (8) amphibole, (9, 10) Cr-diopsides, (11, 12) chromite, (13) mica.

7	8	9	10	11	12	13
–	44.62	54.86	54.73	0.04	0.10	38.39
51.42	0.50	0.37	0.01	0.06	0.38	3.41
0.65	11.31	3.66	2.11	18.37	21.27	12.49
0.78	1.30	1.95	1.39	52.76	48.28	1.47
33.12	3.27	3.06	1.45	17.05	14.81	4.14
0.30	0.02	0.08	0.01	0.29	0.26	0.01
12.19	18.74	14.88	16.25	11.25	13.91	22.46
0.04	10.4	16.28	22.32	0	0.06	0.02
–	3.65	3.60	1.23	0.07	0.03	0.36
0.10	1.51	–	–	–	–	9.88
98.60	95.33	98.74	99.50	99.89	99.11	92.62
0.48	79.1	194	58.9	0.53	0.83	291
0.02	4.8	60.3	35.8	0.024	0.05	2.12
0.043	15.2	102	50.8	0.052	0.25	5.7
0.005	2.6	14.2	7.32	0.009	0.01	0.52
0.041	13.0	54.3	30.6	0.035	0.14	1.65
0.032	2.70	8.2	5.04	0.025	0.07	0.26
0.011	0.82	2.3	1.37	0.024	0.02	0.113
0.046	2.1	5.4	3.51	0.081	0.09	0.202
0.005	0.2	0.7	0.415	0.010	0.011	0.020
0.025	1.1	3.1	1.72	0.025	0.07	0.135
0.003	0.1	0.4	0.24	0.006	0.013	0.015
0.006	0.3	0.9	0.45	0.025	0.02	0.022
0.001	0.03	0.1	0.056	0.003	0.004	0.006
0.015	0.2	0.7	0.24	0.014	0.02	0.026
0.007	0.02	0.1	0.03	0.004	0.01	0.007
5.0	1.7	1.8	1.74	0.017	0.07	0.322
72.9	3.1	0.6	0.26	0.038	0.74	2.184
0.103	0.50	10.7	0.48	0.055	0.203	0.366
0.004	0.096	2.0	2.29	0.003	0.005	0.475
0.006	27.3	0.1	0.28	0.009	0.004	0.324
363	28.2	308	174	294	240	219
11.9	9.8	25.4	18.8	3.9	5.7	6.2
53.8	7553	34.0	18.8	69.9	65.0	59
10.3	5.042	9.5	8.5	8.5	7.2	11.0
6033	170	5931	3795	5762	2010	18368
0.009	3.92	3.0	3.81	0.16	0.562	288
0.78	67.0	502	277	1.2	1.35	10.96
0.034	30.0	13.3	7.29	0.17	0.43	0.57
155	0.01	64.7	37.0	0.85	3.0	11.6
541	0.015	15.3	4.0	0.41	4.74	20.5
0.004	165	0.2	0.17	–	–	2.04

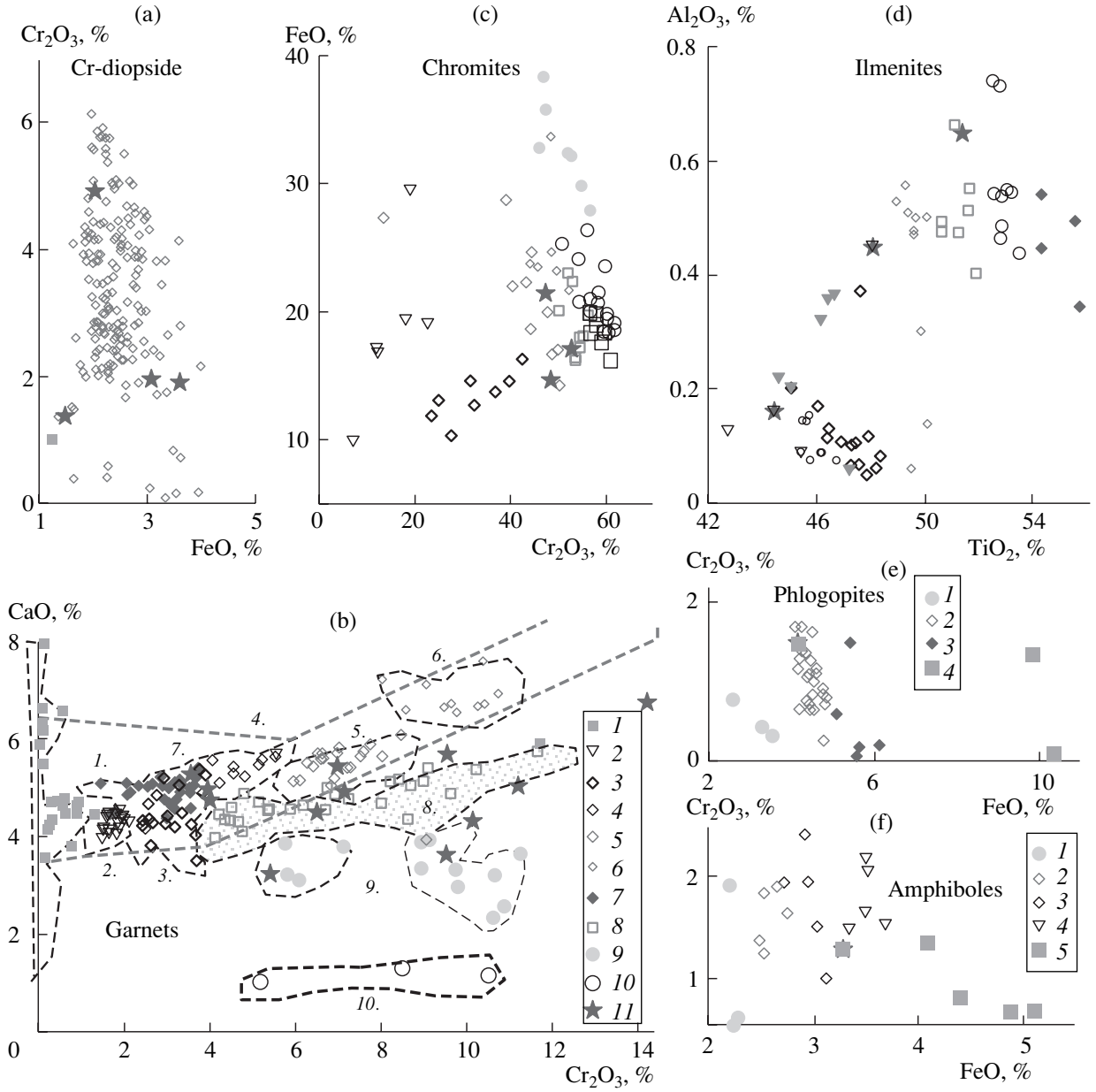

Fig. 1. Compositional variations of different minerals. (a) Clinopyroxenes and (b) garnets from (*1*) megacrysts and pyroxenites, (*2*) Gr–Sp peridotites, (*3*) Gr pyroxenites, (*4*) Gr peridotites, (*5–7*) diamond-facies peridotites, (*8*) depleted (relict) peridotites, (*9*) harzburgites, and (*10*) dunites; (*11*) compositions analyzed by LAM ICP-MS (in all figures); (c) chromites: (*1–9*) groups as for garnets; (d) ilmenites (groups presumably corresponding to depth facies shown in Fig. 2); (e) micas from (*1*) dunites, (*2*) diamond-facies peridotites, (*3*) spinel-facies peridotites, and (*4*) pyroxenites and glimmerites; (f) amphiboles from (*1*) dunites, (*2*) diamond-facies peridotites, (*3*) the middle part of the column, (*4*) spinel-facies peridotites, and (*5*) pyroxenites and metasomatites.

early stages, they formed from protokimberlite melts [6] in magma chambers. A subsequent temperature decrease probably fractionated the primary magma and generated more mobile carbonatites. The final crystallization stages in the mantle were probably related to intense interaction with peridotite column in accord with the AFC mechanism [7] in the branching vein system. When eruptions took place, kimberlite magma ascended along the newly formed channels, reworked the peridotite column and older vein system, and exhumed chemically discrete xenoliths and peridotites. Large-scale metasomatism can result in a change of primary lithological–geochemical features and the multistage formation of nonequilibrium minerals. Thus, compositional series similar to those in the metasomatic column can be produced. This scenario is possible for some peridotites from the Yubileinaya kimberlite field, although primary mineral assemblages are obviously present here. The

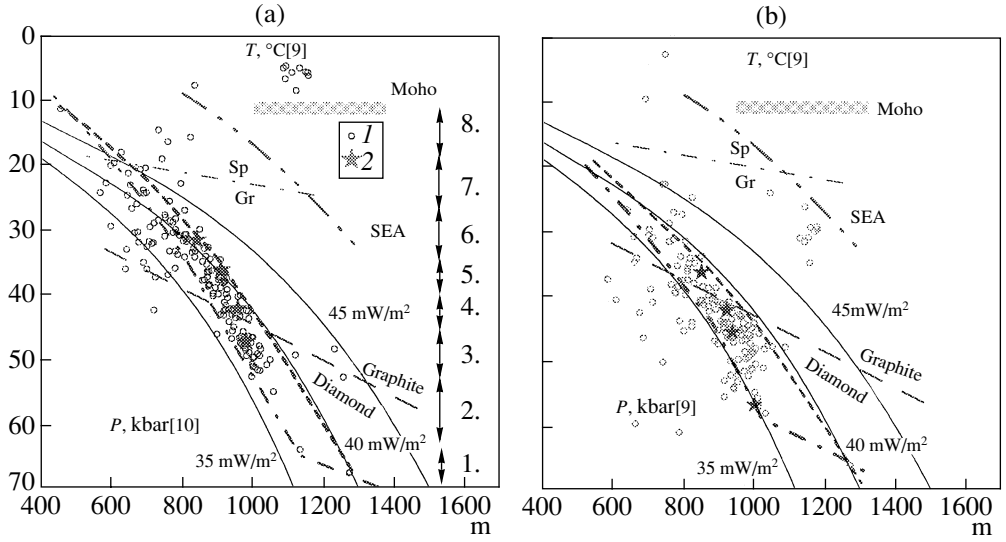

Fig. 2. *TP* diagrams based on clinopyroxene thermobarometry. Temperature and pressure estimates: (a) Based on [9] and [10], respectively, (b) based on [9]. (*1*) Cr-diopsides from concentrate; (*2*) compositions with trace element data based on LAM ICP MS. The identification of eight intervals is based on data point density and facies affiliation.

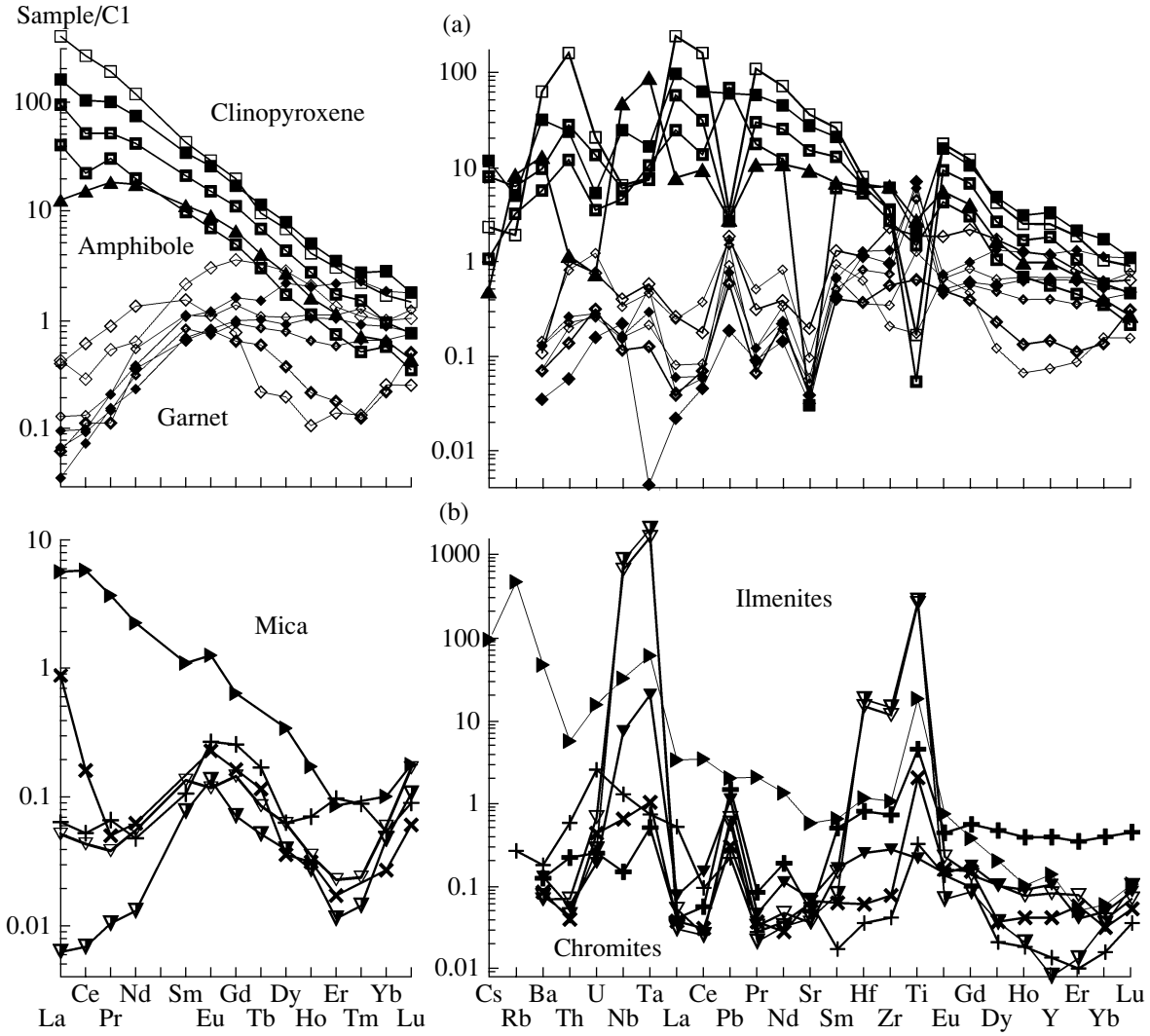

Fig. 3. Chondrite C1-normalized (Evensen, Frost, 1978) REE patterns and PM-normalized spidergrams (McDonough and Sun, 1995). (a) Garnets and Cr-diopsides from the Yubileinaya kimberlite pipe; (b) chromites, ilmenites, and micas.

degree of mantle column metasomatism correlates with that of kimberlite serpentinization.

ACKNOWLEDGMENTS

This work was supported by the Russian Foundation for Basic Research, project nos. 99-05-65688, 00-05-65228, and 03-05-64146.

REFERENCES

1. F. R. Boyd, N. P. Pokhilenko, D. G. Pearson, *et al.*, Contrib. Mineral. Petrol. **128**, 228 (1997).
2. B. L. Beard, K. N. Fraracci, L. A. Taylor, *et al.*, Contrib. Mineral. Petrol. **125**, 293 (1996).
3. I. V. Ashchepkov, N. V. Vladykin, R. H. Mitchell, *et al.*, Dokl. Akad. Nauk **385**, 721 (2002) [Dokl. Earth. Sci. **385A**, 721 (2002)].
4. S. I. Kostrovitskii and D. De Bruin, in *Alkaline Magmatism and Problem of Sources* (Irkutsk, 2001), pp. 170–286 [in Russian].
5. N. V. Sobolev, *Deep-Seated Inclusions in Kimberlites and Problem of the Upper Mantle Composition* (American Geophysical Union, Washington DC, 1977).
6. A. E. Moore, Contrib. Mineral. Petrol. **95**, 245 (1987).
7. D. DePaolo, Earth Planet. Sci. Lett. **53**, 198 (1981).
8. S. Arai, Contrib. Mineral. Petrol. **87**, 260 (1984).
9. P. Nimis and W. R. Taylor, Contrib. Mineral. Petrol. **139**, 541 (2000).
10. I. V. Ashchepkov, Vestn. Ross. Akad. Nauk, No. 1(21), 2003.
11. P. H. Nixon, *Lesotho Kimberlites* (Cape and Transvaal, Cape Town, 1973).
12. I. Leost, T. Stachel, G. P. Brey, *et al.*, Contrib. Mineral. Petrol. **145**, 15 (2003).
13. P. Van Keken, B. Kiefer, and S. M. Peacock, Geochem. Geophys. Geosyst. **3**, 1056 (2002).
14. S. Y. O. O'Reilly, W. L. Griffin, Y. H. Djomani, *et al.* GSA Today **11**, 4 (2001).
15. I. V. Ashchepkov and L. Andre, Geol. Geofiz. **43**, 343 (2002).